

Role of *DOCK8* in Hyper-inflammatory Syndromes

Mingce Zhang, MD, PhD, University of Alabama at Birmingham

Remy R. Cron, high school graduate, University of Alabama at Birmingham

Niansheng Chu, MD, University of Pennsylvania

Junior Nguyen, BS, University of Pennsylvania

Scott M. Gordon, MD, PhD, University of Pennsylvania

Esraa M. Elovely, MD, MSc, Cincinnati Children's Hospital Medical Center, Assiut University

Faculty of Medicine

T. Prescott Atkinson, MD, PhD, University of Alabama at Birmingham

Peter Weiser, MD, University of Alabama at Birmingham

Mark R. Walter, PhD, University of Alabama at Birmingham

Portia A. Kreiger, MD, University of Pennsylvania

Scott W. Canna, MD, University of Pennsylvania

Edward M. Behrens, MD, University of Pennsylvania

Randy Q. Cron, MD, PhD, University of Alabama at Birmingham

Corresponding Author: Randy Q. Cron, MD, PhD, Children's of Alabama, Division of Rheumatology, 1601 7th Ave. S., CPPN, suite G10, Birmingham, AL 35233-1711.

Tel.: (205) 638-9438; FAX: (205) 638-2875; Email: randycron@uabmc.edu

The work was supported by grants from the Histiocytosis Association (to R.Q.C.), the Kaul Pediatric Research Institute (to R.Q.C.), NIH R01-HD-098428 (to S.W.C.), and NIH R01-AI-121250-A1 (to E.M.B.).

ABSTRACT:

Background: Cytokine storm syndromes (CSS), including hemophagocytic lymphohistiocytosis (HLH), are increasingly recognized as hyper-inflammatory states leading to multi-organ failure and death. Familial HLH (FHL) in infancy results from homozygous genetic defects in perforin-mediated cytotoxicity by CD8 T-lymphocytes and natural killer (NK) cells. Later onset CSS are frequently associated with heterozygous defects in FHL genes, but genetic etiologies for most are unknown. We identified rare *DOCK8* variants in CSS patients.

Objective: We explore the role of CSS patient derived *DOCK8* mutations on cytolytic activity in NK cells. We further study effects of *Dock8*^{-/-} in murine models of CSS.

Methods: *DOCK8* cDNA from 2 unrelated CSS patients with different missense mutations were introduced into human NK-92 NK cells by foamy virus transduction. NK cell degranulation (CD107a), cytolytic activity against K562 target cells, and interferon-gamma (IFN γ) production were explored by flow cytometry (FCM). A third CSS patient *DOCK8* mRNA splice acceptor site variant was explored by exon trapping. *Dock8*^{-/-} mice were assessed for features of CSS (weight loss, splenomegaly, hepatic inflammation, cytopenias, and IFN γ levels) upon challenge with lymphochoriomeningitic virus (LCMV) and excess IL-18.

Results: Both patient *DOCK8* missense mutations decreased cytolytic function in NK cells in a partial dominant-negative fashion *in vitro*. The patient *DOCK8* splice variant disrupted mRNA splicing *in vitro*. *Dock8*^{-/-} mice tolerated excess IL-18 but developed features of CSS upon LCMV infection.

Conclusion: Mutations in *DOCK8* may contribute to CSS-like hyper-inflammatory states by altering cytolytic function in a threshold model of disease.

Key Messages

- Heterozygous missense mutations in *DOCK8* may contribute to decreased NK cell function via partial dominant-negative effects on perforin-mediated cytotoxicity.
- Heterozygous mutations in *DOCK8* may contribute to hyper-inflammatory syndromes in a threshold model of disease.
- LCMV infection of *Dock8*^{-/-} mice recapitulates features of murine FHL.

Capsule Summary (≤35 words) – 35 words

Heterozygous missense and splice site mutations in *DOCK8* may contribute to hyper-inflammation in patients with CSS. *DOCK8* is important for optimal NK cell cytotoxic function, and LCMV infection of *Dock8*^{-/-} mice resembles murine FHL.

Key Words: *cytokine storm syndrome, cytotoxicity, degranulation, hemophagocytic lymphohistiocytosis, hyper-inflammation, interferon-gamma, macrophage activation syndrome, missense mutation, natural killer cell, splice site*

Abbreviations used: CSS: cytokine storm syndrome; *DOCK8*: dedicator of cytokinesis 8; FV: foamy virus; HIS: hyper-inflammatory syndrome; HLH: hemophagocytic lymphohistiocytosis; IBD: inflammatory bowel syndrome; LCMV: lymphocytic choriomeningitis virus, MAS: macrophage activation syndrome; NK: natural killer

INTRODUCTION

Hyper-inflammatory syndromes, including hemophagocytic lymphohistiocytosis (HLH) and macrophage activation syndrome (MAS), are frequently fatal conditions resulting from a pro-inflammatory cytokine storm.(1) Familial HLH (FHL) is rare (approximately 1 in 50,000 live births) typically occurring within the first year of life, but secondary forms of HLH (sHLH) may affect up to 1 in 3,000 individuals at any age.(2) FHL results from homozygous autosomal recessive defects in proteins critical for perforin-mediated cytotoxicity by cytotoxic CD8 T-lymphocytes and natural killer (NK) cells.(3) sHLH and MAS are associated with intracellular pathogens (e.g. Epstein-Barr virus (EBV)), hematologic malignancies (e.g. T-cell leukemia), and autoimmune (e.g. systemic lupus erythematosus (SLE)) or autoinflammatory conditions (e.g. systemic juvenile idiopathic arthritis (sJIA)).(4) The distinction between FHL and sHLH is becoming blurred as heterozygous hypomorphic or dominant-negative mutations in FHL genes are being increasingly identified as disrupting NK cell function(5) and contributing to sHLH pathogenesis using a threshold model of disease.(6) As reported, up to 20-40% of sHLH cohorts, possess heterozygous defects in known HLH genes.(7), yet a large percentage of sHLH individuals without known genetic risk factors develop a cytokine storm syndrome (CSS). During the severe acute respiratory syndrome coronavirus 2 (SARS-CoV-2) pandemic up to 20% of infected individuals developed hyper-inflammation requiring hospitalization, and a significant percentage of these hospitalized coronavirus disease 2019 (COVID-19) patients have been identified with heterozygous defects in known FHL genes, but many have not.(8)

Genetic defects in FHL genes as well as in genes associated with primary immunodeficiency (PID) and dysregulated immune activation and proliferation have been found in children with HLH.(9); in this large cohort an affected child was identified with biallelic disruption of the PID gene *DOCK8* (dedicator of cytokinesis 8), not previously associated with HLH.(9)

Homozygous defects in *DOCK8* are known to result in a form of autosomal-recessive Hyper-IgE syndrome.(10) *DOCK8* deficiency may contribute to HLH via disruption of NK cell cytolytic function as demonstrated *in vitro*.(11, 12) *DOCK8* is a GTPase important for cytoskeletal trafficking of granules, including perforin containing cytolytic granules. *DOCK8* also interacts with *CDC42*, a product of another disrupted gene recently identified in patients with HLH(13),it plays multiple roles beyond cytotoxicity, including immune cell migration/trafficking, proliferation, and survival. We propose that heterozygous *DOCK8* mutations may contribute to CSS in sHLH by partially disrupting lymphocyte cytolytic function similar to reports of complete or partial dominant-negative effects on NK cell function resulting from heterozygous mutations in other FHL associated genes identified in sHLH patients,(5, 14-17). Thus, *DOCK8* should be considered as a novel HLH-associated gene.

METHODS

Human subjects

Children with HLH (fulfilling HLH-2004 and/or HScore criteria)(18, 19) hospitalized at Children's of Alabama (Birmingham, AL, USA) have frequently, but not routinely, undergone commercial (GeneDx, Gaithersburg, MD, USA; and Invitae, San Francisco, CA, USA) DNA (exome) sequencing to identify FHL and associated PID genes since September 2007. Between August 2014 and September 2018, 3 of 37 children who underwent DNA sequencing for HLH were noted to have heterozygous mutations in *DOCK8* (Table 1). Upon informed signed consent of subjects/families of a University of Alabama at Birmingham (UAB) Institutional Review Board (IRB) approved protocol, patient peripheral blood mononuclear cell (PBMC) derived mRNA was converted to cDNA to confirm missense mutations by Sanger sequencing, and the splice acceptor site variant was confirmed by targeted genomic DNA sequencing as previously described.(17)

DNA expression constructs

Wild-type (WT) human *DOCK8* expression cDNA was cloned from healthy donor derived PBMC mRNA using reverse transcriptase (ThermoFisher, Waltham, MA, USA) as previously described.(20) Sanger sequence analysis demonstrated the cDNA sequence was equivalent to *DOCK8* mRNA variant 1 (NM_203447). A recombinant Foamy virus (FV) expression system required for more efficient introduction of larger (>5kb) cDNA constructs was kindly provided by Dr. Grant Trobridge at Washington State University (Pullman, WA, USA).(21) This expression system contains the pFV-SGW plasmid expressing the exogenous gene plus enhanced green fluorescent protein (EGFP) driven by the SFFV promoter, as well as 3 helper plasmids that separately produce gag, pol, and env proteins for recombinant viral particle assembly. WT *DOCK8* cDNA was inserted into pFV-SGW to generate the pFV-SGW-*DOCK8*-WT plasmid.(20)

Based on the WT plasmid, the precise HLH patient derived mutant *DOCK8* sequence equivalent cDNAs were generated using a QuikChange Lightning Site-Directed Mutagenesis Kit per the supplied instructions (Agilent Technologies, Santa Clara, CA, USA). The 2 unique patient-derived mutant cDNA were confirmed by Sanger DNA sequence analysis. Recombinant FV preparation and infection of human NK-92 NK cells was conducted as previously described.(20)

NK cell cytolytic and cytokine assays

WT and patient derived *DOCK8*-expressing FV-infected NK-92 cells were independently mixed at effector to target ratios of 1:1 and 5:1 with K562 erythroleukemia cells for 4 hours as detailed previously.(20) For lytic assays, K562 target cells in the absence of NK-92 cells served as a background control. For degranulation (CD107a expression following 1:1 incubation for 0-2 hours with K562 cells) assays, NK-92 cells in isolation served as a background control. Target cell lysis and NK-92 cell degranulation were measured by flow cytometry (FCM) (LSRFortessa, BD Biosciences, Franklin Lakes, NJ) using live/dead fixable cell dead reagent (Invitrogen, Waltham, MA, USA) and anti-CD107a/LAMP1 allophycocyanin (APC)-conjugated antibody (Biolegend, San Diego, CA, USA), respectively, and analyzed with FlowJo 10.2 software (Ashland, OR, USA).(20) FCM intracellular detection of tumor necrosis factor (TNF) and interferon-gamma (IFN γ) of WT and patient derived *DOCK8*-expressing FV-infected NK-92 cells incubated 1:1 with K562 cells for 4 hours was carried out as previously detailed,(17) using fluorochrome-conjugated anti-cytokine antibodies (anti-IFN γ -APC, PharMingen, San Diego, CA, USA; anti-TNF-phycoerythrin (PE), Biolegend), anti-granzyme B-APC, and isotype controls (eBioscience, San Diego, CA, USA) in the presence of brefeldin A (golgi retention) and saponin (permeabilization).(22) K562 cells were labeled with eFluor 670 dye (Invitrogen, Waltham, MA).

Splice variant reporter gene constructs

The modified EGFP reporter plasmids were constructed using traditional cloning methodologies as follows: protocol one (developed novel assay), the EGFP cDNA was spliced into the equivalent of 2 in-frame “exons” – EGFP 1/2 (1-336 bp) and EGFP 2/2 (337-720 bp); a centrally truncated *DOCK8* intron 1 (416 bp, containing the 5’ and 3’ regions of the intron) – either WT 3’ splice acceptor site variant or patient derived mutation was inserted between the EGFP “exons”, as shown in Fig 2, A. For protocol two (standard exon trapping plasmid assay), the first 2 *DOCK8* exons (53 bp and 103 bp in length, respectively) plus the EGFP cDNA serve as multiple exons; shortened introns from *DOCK8* (either WT or mutant 3’ splice acceptor site of *DOCK8* intron 1, 359 bp, and *DOCK8* intron 2, 783 bp in length) were inserted in frame between the 3 exons, as shown in Fig 2, D. The plasmids were electroporated into NK-92 cells using a 4D-Nucleofector (Lonza, Basel, Switzerland) according to the manufacturer’s instructions. GFP expression was detected by FCM.

Small interfering RNA (siRNA) studies

For *DOCK8* mRNA knockdown, the indicated amounts (Fig 3: 500 nM total per condition, with increasing amounts of *DOCK8* siRNA relative to control siRNA) of 3-Dicer substrate *DOCK8* siRNAs mixture (TriFECTa *DOCK8* siRNA kit, purchased from Integrated DNA Technologies, IDT, San Diego, CA) were nucleofected (Lonza) into 2×10^6 NK-92 cells.(23) Dose-dependent diminished *DOCK8* mRNA levels were confirmed with ~90% reduction of *DOCK8* expression at maximal *DOCK8* siRNA concentration compared with the negative control as detected by qPCR at 24 hours after transfection (data not shown). The transfected cells were used to test for cytolysis and degranulation 24 hours post-transfection as described above.

CRISPR/Cas9 genetic alterations

DOCK8 genomic editing was performed by using CRISPR(cr)/Cas9 technology.(24) Briefly, *DOCK8* specific crRNA targeting the sequences (150 bp) in the vicinity of the patient 1 mutation (c.792T) was designed by using the IDT online service tool (CRISPR/Cas9 guide (g)RNA checker) and purchased from IDT. The most efficient, most specific, and with least off-target gRNA sequences were chosen (gel electrophoresis, data not shown). The crRNA and tracrRNA were first annealed to form the gRNA–ctRNA complex, followed by addition of Cas9 (Cas9-3NLS-v2, from IDT) to form the complete complex of Cas9–gRNA–ctRNA. The complex was nucleofected into NK-92 cells using a 4D-nucleofector (Lonza) according to the manufacturer's instructions. An 88 bp enhancer oligonucleotide or 98 bp single stranded template oligonucleotide (ssODN, purchased from IDT) was also used during the transfection. Targeting of *DOCK8* genomic DNA was confirmed by gel electrophoresis (data not shown). Transfected NK-92 cells were then studied for cytolysis and degranulation in the presence of K562 cells as described above.

Mice studies

WT C57BL/6J mice were obtained from Jackson Laboratories (Bar Harbor, ME, USA). *Dock8*^{-/-} and *I18tg* mice were generous gifts from Dr. Helen Su (National Institutes of Health, Bethesda, MD, USA)(25) and Dr. Tomoaki Hoshino (Kurume University),(26) respectively. All experimental mice were age matched. All experiments were conducted in accordance with national guidelines and approved by the Institutional Animal Care and Use Committee (IACUC) of the Children's Hospital of Philadelphia. For LCMV infection, 2 x 10⁶ PFU of Armstrong strain LCMV was injected intraperitoneally into mice ages 6-8 weeks. Mice were weighed daily after infection. Cheek bleeding was used to obtain peripheral blood on day 0 and day 8 of infection for complete blood count analysis. Mice were euthanized on day 8. Spleens and livers were

harvested for downstream analysis, and serum was obtained. For peripheral blood counts, 200 μ L of peripheral blood was analyzed on a Sysmex XT-2000iV Hematology Analyzer (Kobe, Hyogo, Japan) to obtain white blood cell, red blood cell, and platelet counts. For detailed white blood cell analysis, red blood cells were lysed with ammonium-chloride-potassium (ACK) buffer, leukocytes stained with antibodies against B220, CD90, Ly-6G, NK1.1, TCR β , CD4, CD8, and PD-1 (BD Pharmingen), cells assessed by flow cytometry, and data analyzed in FlowJo v10 (Treestar). Serum soluble CD25 (sCD25) and IFN γ were measured by ELISA using OptEIA kits (PharMingen) according to manufacturer's protocol. Liver histology sections were fixed in formalin, embedded in paraffin, and stained with hematoxylin and eosin. A blinded pathologist (PAK) read the slides for lobular and portal inflammation, and endothelialitis according to published methods and scoring scales.(27)

Statistics

Statistical analyses were performed with GraphPad Prism (GraphPad Software, La Jolla, CA, USA) software as described in figure legends.

RESULTS

Case presentation:

A teen male (Table 1, patient 1), presented to the hospital with fever, headache, vomiting, non-bloody diarrhea, and abdominal pain for 4 days preceded by upper respiratory tract symptoms for 2 days. He developed acute respiratory distress syndrome (ARDS) requiring mechanical ventilation. Hepatosplenomegaly was noted on exam, and laboratory findings revealed bicytopenia, liver dysfunction, coagulopathy, hyperferritinemia, elevated sCD25, and greatly diminished NK cell lytic function (Table 2). The patient satisfied 7 out of the 8 HLH-2004 criteria(19) and met the HScore threshold(18) to diagnose HLH. An extensive infectious workup revealed *Bartonella henselae* infection by serology. Genetic sequence analysis showed a heterozygous novel mutation in the *DOCK8* gene (c.782C>T, p.Ala261Val) and was negative for FHL genes. *DOCK8* A261V is a conservative amino acid substitution, but *in silico* analysis predicts this variant is damaging to the protein structure/function. The mutation was predicted to be likely pathogenic by PolyPhen-2 (Table 1).

Two additional patients with HLH diagnosed by HLH-2004 and/or HScore criteria were identified with heterozygous *DOCK8* mutations and no variants in FHL genes. Patient 2 (Table 1) was a teen boy with juvenile idiopathic arthritis (JIA, enthesitis related arthritis (ERA) subtype) with a rare *DOCK8* missense mutation (c.4850A>G, p.Gln1617Arg) considered to be possibly pathogenic. Patient 3, a teen male, developed HLH (7/8 HLH-2004 criteria) (Table 2) in the setting of ongoing treatment for T-cell leukemia. He was noted to have a *DOCK8* splice acceptor site mutation (c.54-1G>T) that was considered likely pathogenic (Table 1). All 3 HLH patients with heterozygous *DOCK8* mutations survived their hospitalizations, with patient 1 responding to antibiotics and patients 2 and 3 responding to IL-1 blockade (anakinra) and glucocorticoids.

Heterozygous HLH patient-derived *DOCK8* missense mutations partially disrupt NK cell function

To explore the role of the heterozygous *DOCK8* mutations from patient 1 and patient 2, a lentiviral expression construct was generated that co-expressed EGFP and WT (control) or mutant (c.782C or c.4850A) *DOCK8* cDNA. Human NK-92 cells, which natively express both WT *DOCK8* and the machinery for perforin-mediated cytotoxicity(17), were transduced with *DOCK8* expressing WT or patient-derived FV as in the Methods. NK cell lytic activity of the *DOCK8* c.782T (patient 1) expressing NK-92 cells was approximately half that compared to WT *DOCK8* (c.782C) expressing cells. (Fig 1, A and B). Similarly, degranulation by *DOCK8* c.782T expressing NK-92 cells was nearly half that of WT NK-92 cells (Fig 1, C and D). The decreased killing was not due to decreased granzyme B levels (Fig E1), but perhaps related to an appreciable decreased level of conjugate formation between NK-92 cells and the K562 target cells at later time points (30-60 minutes) post-mixing (Fig E2), as has been noted previously in *DOCK8* deficiency.(28) Similar less robust, but statistically significant, reduction in NK cell lysis and degranulation was noted for the patient 2 derived *DOCK8* c.4850A>G mutation (Fig E3, A-D). Thus, the FV introduced patient derived *DOCK8* mutations function as partial-dominant negatives (in the presence of NK-92 WT *DOCK8* germline genes) to inhibit NK cell lytic function.

We and others have previously shown the complete absence or partial disruption of genes in the perforin-mediated cytotoxic pathway leads to delayed granule polarization to the immunologic synapse, diminished or absent killing, and prolonged engagement between the lytic lymphocyte (NK cell or CD8 T-cells) and its target cell.(17, 29, 30) The prolonged engagement is associated with increased pro-inflammatory cytokine production believed to contribute to the HLH.(17, 29, 30) NK-92 cells expressing WT (c.782C) or the patient 1 derived *DOCK8* mutation (c.782T) were studied for intracellular cytokine expression following incubation

with K562 target cells. NK-92 cells expressing the *DOCK8* c.782T mutation produced approximately 3-fold more intracellular TNF and 2-fold more intracellular IFN γ compared to WT cells (Fig 1, E and F). This resembles the increased IFN γ production seen by a partial dominant-negative heterozygous *RAB27A* mutation identified in 2 unrelated teenagers with sHLH.(17)

A HLH patient-derived splice acceptor site mutation disrupts *DOCK8* mRNA splicing

The heterozygous mutation in *DOCK8* (c.54-1G>T) from HLH patient 3 (Table 1) was in a predicted splice acceptor site at the 3' end of intron 1. To explore the effect of the mutation functionally, we developed a novel plasmid-based assay. Using standard cloning techniques, we modified a standard EGFP expression plasmid (see Methods) in which the EGFP cDNA was interrupted in frame by inserting *DOCK8* intron 1 possessing the WT (c.54-1 G) or the patient derived mutation (c.54-1 T) at the 3' splice acceptor site, as if the EGFP cDNA was 2 exons separated by an intron. Thus, correct splicing out of intron 1 from *DOCK8* would be required to generate EGFP RNA and subsequent protein to be detected by FCM.

Experimentally, EGFP expression plasmids were introduced into NK-92 cells by transfection, and the cells were placed back into culture. EGFP protein expression was screened by FCM at 1- and 3-days post-transfection. NK-92 cells transfected with the EGFP expression plasmid containing the EGFP cDNA disrupted by the *DOCK8* intron 1 WT sequence (Fig 2, A) expressed similar levels of EGFP as the intact parent EGFP expression plasmid (Fig 2, B), but NK-92 cells transfected with the EGFP expression plasmid containing the EGFP cDNA disrupted by the *DOCK8* intron 1 patient 3-derived mutation at the 3' splice acceptor site (Fig 2, A) had minimal EGFP expression (Fig 2, B). Averaged over 4 separate experiments, NK-92 cells transfected with the WT *DOCK8* intron 1 expressed roughly equivalent levels as those cells expressing the parent EGFP expression plasmid (Fig 2, C), but NK-92 cells transfected

with the EGFP plasmid containing the *DOCK8* intron 1 patient 3-derived mutation at the 3' splice acceptor site had approximately 80-90% reduction in GFP expression (Fig 2, C). This argues that the patient-derived mutation at the 3' end of *DOCK8* intron 1 is required for optimal mRNA splicing and subsequent *DOCK8* protein expression.

We confirmed these results by the more traditional and established plasmid-based exon trapping assay,(31) in which *DOCK8* exon 1 and 2, separated by WT or patient mutation intron 1, were subcloned in frame and upstream of EGFP cDNA to provide more representative mRNA splicing context (Fig 2, D). Similar to the results of our own EGFP plasmid-based assay, NK-92 cells expressing the *DOCK8* intron 1 mutant splice acceptor nucleotide had drastically diminished EGFP expression compared to those expressing the WT nucleotide (Fig 2, E and F). Thus, it is possible that HLH patient-derived heterozygous mutations may contribute to altered NK cell function by dominant-negative (Fig 1) or potentially hypomorphic effects (Fig 2).

Decreased *DOCK8* expression diminishes NK cell cytolytic function

To explore the effect of diminished *DOCK8* expression on NK cell function, two complimentary approaches were undertaken. First, increasing amounts of *DOCK8*-specific siRNA were introduced into NK-92 cells by transfection. NK-92 cells were then assayed for lytic activity versus K562 target cells, and degranulation in the presence of stimulating K562 cells. Relative to scrambled siRNA control, increasing quantities of *DOCK8*-targeted siRNA reduced both killing and degranulation in a dose-dependent fashion as detected by FCM (Fig 3, A and Fig 3, C, respectively). Averaged over 4 independent experiments, knockdown of *DOCK8* message statistically significantly reduced NK cell lysis by approximately 40% (Fig 3, B) and reduced degranulation (CD107a expression) by approximately 30% (Fig 3, D) at the highest

concentration of *DOCK8* siRNA (80-90% reduction of *DOCK8* siRNA by RT-PCR, data not shown).

As an alternative approach, *DOCK8* message was disrupted by targeting genomic *DOCK8* DNA, using *DOCK8*-specific guide RNA, within NK-92 cells by CRISPR/Cas9 technology. Disruption of *DOCK8* on both alleles resulted in approximately 50% reduction in NK cell lytic activity (Fig 4, A) and degranulation (Fig 4, C) as detected by FCM in a statistically significant manner averaged over 4 independent experiments (Fig 4, B and D). This argues that *DOCK8* is required for optimal NK cell lytic activity but is not absolutely required for killing/degranulation. Re-introduction of WT *DOCK8* DNA (c.782C) by CRISPR/Cas9 restored both K562 lysis and degranulation, whereas introduction of the patient 1 *DOCK8* mutation (c.782T) was no better at NK cell lysis/degranulation than disrupted *DOCK8* (Fig 4). This provides further evidence the patient 1 *DOCK8* missense mutation disrupts NK cell lytic function.

LCMV infection of *DOCK8* deficient mice leads to hyper-inflammation resembling HLH

To explore the role of *DOCK8* in NK cell function *in vivo*, WT and *Dock8*^{-/-} mice (32) were infected with LCMV as originally modelled in *Prf1*^{-/-} mice.(33) After 4 days of infection, the B6 WT animals began to gain back body weight, whereas the *Dock8*^{-/-} animals continued to lose weight until day 8 euthanization as required by protocol (Fig 5, A). As typically seen in humans and mice with HLH,(34) splenomegaly was noted in the LCMV infected *Dock8*^{-/-} mice (Fig 5, B). Liver pathology was also noted, as often seen in human HLH, with increased endothelial activation (Fig E4). In addition, thrombocytopenia was noted in *Dock8*^{-/-} mice relative to WT animals following LCMV infection (Fig 5, D), but no other relative cytopenias were identified (Fig 5, C and D). Serum IFN γ levels were slightly elevated in *Dock8*^{-/-} mice compared to WT mice (Fig 5, E), similar but not as severe as in LCMV infected *Prf1*^{-/-} animals.(33) Another common

HLH feature (4) and marker of lymphocyte activation, elevation of serum sCD25, was not seen in *Dock8*^{-/-} mice compared to WT controls (Fig 5, E). Lastly, and similar to *Prf1*^{-/-} animals,(33) the *Dock8*^{-/-} mice did not clear the LCMV infection as well in comparison to WT mice (Fig 5, F). Thus, consistent with *in vitro* disruption of *DOCK8*, in which *DOCK8* disruption is not as severe as would be seen in *PRF1* disruption (Fig 3 and Fig 4),(35, 36) LCMV infection of *Dock8*^{-/-} mice leads to a hyper-inflammatory HLH-like state that is not as severe as in *Prf1*^{-/-} animals.(33)

We recently have demonstrated synergy between cytotoxic impairment (perforin deficiency) and autoinflammation in the form of excess IL-18 (*Il18tg*) in driving spontaneous murine HLH.(37) To determine its interactions with excess IL-18, *Dock8*^{-/-} mice were crossed with *Il18tg* mice and studied for HLH features. *Dock8*^{-/-}; *Il18tg* animals developed minimal evidence of spontaneous HLH, with trends towards increased spleen size and NK cytopenia (Fig 6, A). Using PD1 expression as a marker of CD8 T-cell hyperactivation,(38) *Dock8*^{-/-} mice showed CD4 and CD8 lymphopenia, whereas excess IL-18 rescued CD8 lymphopenia with an increase in activated CD8 T-cells (Fig 6, A). Similar, but more overwhelming, increases in hyperactivated CD8 T-cells were observed in human HLH/MAS(39, 40) and in *Prf1*^{-/-}; *Il18tg* mice.(38) When infected with LCMV, *Dock8*^{-/-}; *Il18tg* mice displayed slightly more weight loss, anemia, neutropenia, and thrombocytopenia (data not shown) than *Dock8*^{-/-} or *Il18tg* alone (Fig 6, B). Nearly all CD8 T-cells were hyperactivated (PD1+), but they were less abundant, likely reflecting *Dock8*-deficiency's effect on CD8 T-cell survival (Fig 6, B).(41) The combination of the cytolytic impairment (*Dock8*^{-/-}) and autoinflammation (*Il18tg*) in the setting of an infectious trigger (LCMV) supports the development of CSS using a threshold model of disease.(16)

DISCUSSION

FHL typically presents in infancy resulting from homozygous defects in genes critical for perforin-mediated cytotoxicity.(42) Many (30-40%) of older children and adults with CSS, like HLH and MAS possess heterozygous defects in these well-established FHL genes(42) with partial or complete dominant-negative effects(43-45) leading to sHLH.(45, 46) However, there are CSS patients with defects in NK cell lytic function (e.g. patients 1 and 2, [Table 1](#)) without identified defects in known perforin pathway genes. We identified heterozygous *DOCK8* mutations in 3 young patients with sHLH without perforin pathway gene mutations. Two of them (patients 1 and 2) displayed defective NK cell function ([Table 2](#)) and had novel or rare *DOCK8* missense mutations ([Table 1](#)) resulting in partial defects in NK/cytotoxic T-cell killing ([Fig 1](#) and [Fig E3](#)) likely contributing to the CSS in a partial-dominant negative fashion using a threshold model of disease.(6)

In such an additive threshold model, a genetic contribution to partial NK cell cytotoxic function results in increased pro-inflammatory cytokine levels, which when added to the inflammation from an underlying condition, e.g. leukemia or systemic lupus erythematosus, and/or certain infectious triggers (e.g. EBV) may reach a threshold at which the host immune response can no longer tolerate the “cytokine storm” and contributes to the multiorgan system disruption.(6, 47) This model helps to explain how relatively subtle genetic defects in lymphocyte lytic function may normally be tolerated but contribute to CSS under certain conditions.(15) Homozygous genetic defects in perforin pathway genes require very little stimulus to overcome an immune balance threshold, but heterozygous defects that partially alter lymphocyte cytotoxicity may contribute to overcoming the CSS threshold in various heightened inflammatory settings.

Patient 1, with a heterozygous, likely pathogenic, and novel missense mutation in *DOCK8* developed sHLH in the setting of an infectious trigger, *Bartonella henselae* ([Table 1](#)). The intracellular pathogen, *Bartonella* has been reported in association with sHLH in 2 cases with

underlying renal transplantation.(48, 49) By comparison, patient 2, with a heterozygous, possibly pathogenic, rare missense *DOCK8* mutation, developed CSS in the setting of a JIA/ERA disease flare (Table 1). Of note, we have formerly reported 2 children who developed sHLH with partial dominant-negative mutations in *RAB27A* and *UNC13D*, respectively, who both went on to develop JIA/ERA.(17, 50) Thus, the threshold model of disease may help explain how partial defects in lymphocyte cytotoxicity from heterozygous missense mutations in *DOCK8* (Fig 1 and Fig E3, respectively) contribute to sHLH development in the context of an intracellular pathogen (Table 1, patient 1) or an autoimmune disease flare (Table 1, patient 2). Recently, we reported 4 out of 39 children with the post-COVID-19 MIS-C, multisystem inflammatory syndrome in children (MIS-C),(51) who possessed unique *DOCK8* missense mutations, all with partial dominant-negative effects on NK cell lytic function.(20) We are currently exploring the function of 3 unique *DOCK8* missense mutations from 20 severe COVID-19 adults who underwent genetic sequencing as part of a clinical trial.(52)

In contrast to patients 1 and 2, the rare, likely pathogenic *DOCK8* mutation from patient 3 (Table 1) yielded a splice acceptor site defect that disrupted RNA splicing (Fig 2). A heterozygous hypomorphic defect may or may not have contributed to CSS development in patient 3, who suffered from T-cell leukemia (a known HLH trigger)(53) and a potential *Candida* infectious trigger in the setting of iatrogenic immunodeficiency.(54) Nevertheless, heterozygous hypomorphic defects in FHL genes may contribute to sHLH development.(55) As *DOCK8* does not appear to be absolutely required for NK cell lytic function (Fig 4), the contribution of a heterozygous hypomorphic mutation in *DOCK8* to CSS may be difficult to establish. Nonetheless, peak *DOCK8* levels appear to be required for optimal NK cell cytotoxic activity (Fig 3). Moreover, a prior report details a heterozygous splice donor site mutation in *DOCK8* contributing to impaired lymphocyte cytotoxicity.(56) Thus, heterozygous hypomorphic *DOCK8* genetic defects may contribute to CSS in a threshold model of disease.(6)

By comparison, homozygous disruption of *DOCK8*, results in more severe defective NK cell lytic function in humans(11, 12) and homozygous *DOCK8* deficiency was reported to be associated with HLH in a child.(9) Herein, we studied a murine model of FHL by infecting *Dock8*^{-/-} mice with LCMV (Fig 5) and noted a HIS resembling, but not as severe as, LCMV infected *Prf1*^{-/-} animals.(33) While LCMV infected *Dock8*^{-/-} mice, in comparison to WT animals, did not clear infection well, and had features of sHLH (splenomegaly, thrombocytopenia, liver inflammation) (Fig 5 and Fig E4), they only had minimally elevated levels of IFN γ (Fig 5, E). Perhaps, this relates to the importance of DOCK8 in lymphocyte cytokine production,(11) such that there is a trade-off between a cytokine production defect(57, 58) and increased cytokine production resulting from prolonged interaction between defective lytic lymphocytes and their stimulating infected target cells.(29, 30) This may help explain why children with Hyper-IgE syndrome secondary to DOCK8 deficiency are not commonly reported to develop CSS.(59) Nevertheless, the addition of autoinflammation (*Il18tg*) on top of the cytolytic defect (*Dock8*^{-/-}) contributes to a more severe HIS in the LCMV infection model of murine HLH (Fig 6).

The mechanism by which heterozygous *DOCK8* missense mutations disrupt NK cell cytolytic activity is not entirely clear. Others have shown that disruption in DOCK8 has no effect on intracellular perforin levels,(57, 58) and we show that the patient 1 *DOCK8* missense mutation has no effect on granzyme B levels (Fig E1) despite the partial dominant-negative effect on NK cell cytolytic activity (Fig 1). Others have reported that DOCK8 is not required for NK cell conjugation with its target cell(11), but our data suggest that a partial dominant-negative *DOCK8* missense mutation may subtly diminish conjugate formation (Fig E2). The ability of DOCK8 to activate CDC42, together with Wiskott-Aldrich syndrome protein, is critical for coordinated F-actin reorganization and proper formation of the lytic immunologic synapse between NK cells and their target cells.(12) Thus, partial dominant-negative missense mutations in *DOCK8* may delay cytolytic granule trafficking to the immunologic synapse as has been shown for a partial

dominant-negative missense mutation in *RAB27A* identified in 2 unrelated children with sHLH. Exactly how a partial dominant-negative *DOCK8* missense mutation would alter CDC42 (a newly described HLH related gene)(13) activation and subsequent actin-dependent cytolytic granule movement is unclear, as *in silico* modeling of the patient 1 and patient 2 *DOCK8* missense mutations does not predict a direct disrupted interaction with CDC42 (data not shown) based on crystal structure data.(60) Nonetheless, both patient-derived *DOCK8* missense mutations partially disrupt NK cell cytotoxicity (Fig 1 and Fig E3) and likely contributed to sHLH development.

CONCLUSIONS

Herein, we describe 3 individuals with sHLH, all with heterozygous mutations in the primary immunodeficiency gene, *DOCK8*, which is well known to be required for optimal NK cell cytolytic function. We demonstrate the 2 *DOCK8* missense mutations inhibit NK cell lysis and degranulation when introduced into NK-92 cells via FV. The other *DOCK8* mutation, altering a splice acceptor site nucleotide, was shown to disrupt RNA splicing using a novel and an established reporter gene electroporated into NK-92 cells. Stepwise (siRNA) or complete disruption (CRISPR/Cas9) of *DOCK8* in NK-92 cells substantially diminished NK cell lytic function but does not appear to be absolutely required. Lastly, LCMV infection of *Dock8*^{-/-} mice resembles murine HLH but is not as severe as traditional FHL mouse models. Taken together, we propose that *DOCK8* be considered a sHLH associated gene.

ACKNOWLEDGMENTS

We thank the patients and their families for participation in these studies.

COMPETING INTERESTS

R.Q.C. and E.M.B. have received clinical trial grant support and consulting fees from Sobi (manufacturer of anakinra). R.Q.C. and S.W.C. received speaking fees from Sobi and Practicepoint, CME. There are no other relevant financial disclosures.

REFERENCES

1. Canna SW, Cron RQ. Highways to hell: mechanism based management of Cytokine Storm Syndromes. *J Allergy Clin Immunol*. 2020;146:949-59.
2. Jordan MB, Allen CE, Weitzman S, Filipovich AH, McClain KL. How I treat hemophagocytic lymphohistiocytosis. *Blood*. 2011;118(15):4041-52.
3. Janka GE. Familial and acquired hemophagocytic lymphohistiocytosis. *Annu Rev Med*. 2012;63:233-46.
4. Henderson LA, Cron RQ. Macrophage Activation Syndrome and Secondary Hemophagocytic Lymphohistiocytosis in Childhood Inflammatory Disorders: Diagnosis and Management. *Paediatr Drugs*. 2020;22(1):29-44.
5. Zhang M, Behrens EM, Atkinson TP, Shakoory B, Grom AA, Cron RQ. Genetic defects in cytolysis in macrophage activation syndrome. *Curr Rheumatol Rep*. 2014;16(9):439-46.
6. Strippoli R, Caiello I, De Benedetti F. Reaching the threshold: a multilayer pathogenesis of macrophage activation syndrome. *J Rheumatol*. 2013;40(6):761-7.
7. Rocco JM, Laidlaw E, Galindo F, Anderson M, Sortino O, Kuriakose S, et al. Mycobacterial Immune Reconstitution Inflammatory Syndrome in HIV is Associated With Protein-Altering Variants in Hemophagocytic Lymphohistiocytosis-Related Genes. *J Infect Dis*. 2023;228(2):111-5.
8. Schulert GS, Blum SA, Cron RQ. Host genetics of pediatric SARS-CoV-2 COVID-19 and multisystem inflammatory syndrome in children. *Curr Opin Pediatr*. 2021;33(6):549-55.
9. Chinn IK, Eckstein OS, Peckham-Gregory EC, Goldberg BR, Forbes LR, Nicholas SK, et al. Genetic and mechanistic diversity in pediatric hemophagocytic lymphohistiocytosis. *Blood*. 2018;132(1):89-100.
10. Su HC, Jing H, Angelus P, Freeman AF. Insights into immunity from clinical and basic science studies of DOCK8 immunodeficiency syndrome. *Immunol Rev*. 2019;287(1):9-19.
11. Kearney CJ, Vervoort SJ, Ramsbottom KM, Freeman AJ, Michie J, Peake J, et al. DOCK8 Drives Src-Dependent NK Cell Effector Function. *J Immunol*. 2017.
12. Mizesko MC, Banerjee PP, Monaco-Shawver L, Mace EM, Bernal WE, Sawalle-Belohradsky J, et al. Defective actin accumulation impairs human natural killer cell function in patients with dedicator of cytokinesis 8 deficiency. *J Allergy Clin Immunol*. 2013;131(3):840-8.
13. Lam MT, Coppola S, Krumbach OHF, Prencipe G, Insalaco A, Cifaldi C, et al. A novel disorder involving dyshematopoiesis, inflammation, and HLH due to aberrant CDC42 function. *J Exp Med*. 2019;216(12):2778-99.
14. Reiff DD, Zhang M, Smitherman EA, Mannion ML, Stoll ML, Weiser P, Cron RQ. A Rare STXBP2 Mutation in Severe COVID-19 and Secondary Cytokine Storm Syndrome. *Life (Basel)*. 2022;12(2).
15. Schulert GS, Zhang M, Fall N, Husami A, Kissell D, Hanosh A, et al. Whole-Exome Sequencing Reveals Mutations in Genes Linked to Hemophagocytic Lymphohistiocytosis and Macrophage Activation Syndrome in Fatal Cases of H1N1 Influenza. *J Infect Dis*. 2016;213(7):1180-8.
16. Spessott WA, Sanmillan ML, McCormick ME, Patel N, Villanueva J, Zhang K, et al. Hemophagocytic lymphohistiocytosis caused by dominant-negative mutations in STXBP2 that inhibit SNARE-mediated membrane fusion. *Blood*. 2015;125(10):1566-77.
17. Zhang M, Bracaglia C, Prencipe G, Bemrich-Stolz CJ, Beukelman T, Dimmitt RA, et al. A heterozygous RAB27A mutation associated with delayed cytolytic granule polarization and hemophagocytic lymphohistiocytosis. *J Immunol*. 2016;196(6):2492-503.
18. Fardet L, Galicier L, Lambotte O, Marzac C, Aumont C, Chahwan D, et al. Development and validation of a score for the diagnosis of reactive hemophagocytic syndrome (HScore). *Arthritis Rheumatol*. 2014;66(9):2613-20.

19. Henter JI, Horne A, Arico M, Egeler RM, Filipovich AH, Imashuku S, et al. HLH-2004: Diagnostic and therapeutic guidelines for hemophagocytic lymphohistiocytosis. *Pediatr Blood Cancer*. 2007;48(2):124-31.
20. Vagreicha A, Zhang M, Acharya S, Lozinsky S, Singer A, Levine C, et al. Hemophagocytic Lymphohistiocytosis Gene Variants in Multisystem Inflammatory Syndrome in Children. *Biology (Basel)*. 2022;11(3).
21. Trobridge GD. Foamy virus vectors for gene transfer. *Expert Opin Biol Ther*. 2009;9(11):1427-36.
22. Zhang M, Clausell A, Robinson T, Yin J, Chen E, Johnson L, et al. Host factor transcriptional regulation contributes to preferential expression of HIV type 1 in IL-4-producing CD4 T cells. *J Immunol*. 2012;189(6):2746-57.
23. Yin J, Ma Z, Selliah N, Shivers DK, Cron RQ, Finkel TH. Effective gene suppression using small interfering RNA in hard-to-transfect human T cells. *J Immunol Methods*. 2006;312(1-2):1-11.
24. Jacobi AM, Rettig GR, Turk R, Collingwood MA, Zeiner SA, Quadros RM, et al. Simplified CRISPR tools for efficient genome editing and streamlined protocols for their delivery into mammalian cells and mouse zygotes. *Methods*. 2017;121-122:16-28.
25. Randall KL, Lambe T, Johnson AL, Treanor B, Kucharska E, Domaschew H, et al. Dock8 mutations cripple B cell immunological synapses, germinal centers and long-lived antibody production. *Nat Immunol*. 2009;10(12):1283-91.
26. Hoshino T, Kawase Y, Okamoto M, Yokota K, Yoshino K, Yamamura K, et al. Cutting edge: IL-18-transgenic mice: in vivo evidence of a broad role for IL-18 in modulating immune function. *J Immunol*. 2001;166(12):7014-8.
27. Biswas C, Chu N, Burn TN, Kreiger PA, Behrens EM. Amelioration of Murine Macrophage Activation Syndrome by Monomethyl Fumarate in Both a Heme Oxygenase 1-Dependent and Heme Oxygenase 1-Independent Manner. *Arthritis & rheumatology*. 2021;73(5):885-95.
28. Ham H, Guerrier S, Kim J, Schoon RA, Anderson EL, Hamann MJ, et al. Deducator of cytokines 8 interacts with talin and Wiskott-Aldrich syndrome protein to regulate NK cell cytotoxicity. *J Immunol*. 2013;190(7):3661-9.
29. Anft M, Netter P, Urlaub D, Prager I, Schaffner S, Watzl C. NK cell detachment from target cells is regulated by successful cytotoxicity and influences cytokine production. *Cell Mol Immunol*. 2020;17(4):347-55.
30. Jenkins MR, Rudd-Schmidt JA, Lopez JA, Ramsbottom KM, Mannering SI, Andrews DM, et al. Failed CTL/NK cell killing and cytokine hypersecretion are directly linked through prolonged synapse time. *J Exp Med*. 2015;212(3):307-17.
31. Tompson SW, Young TL. Assaying the Effects of Splice Site Variants by Exon Trapping in a Mammalian Cell Line. *Bio Protoc*. 2017;7(10).
32. Zhang Q, Dove CG, Hor JL, Murdock HM, Strauss-Albee DM, Garcia JA, et al. DOCK8 regulates lymphocyte shape integrity for skin antiviral immunity. *J Exp Med*. 2014;211(13):2549-66.
33. Jordan MB, Hildeman D, Kappler J, Marrack P. An animal model of hemophagocytic lymphohistiocytosis (HLH): CD8+ T cells and interferon gamma are essential for the disorder. *Blood*. 2004;104(3):735-43.
34. Lee PY, Cron RQ. The Multifaceted Immunology of Cytokine Storm Syndrome. *J Immunol*. 2023;210(8):1015-24.
35. Behrens EM, Cron RQ. Kill or be killed. *J Immunol*. 2015;194(11):5041-3.
36. Stepp SE, Dufourcq-Lagelouse R, Le Deist F, Bhawan S, Certain S, Mathew PA, et al. Perforin gene defects in familial hemophagocytic lymphohistiocytosis. *Science*. 1999;286(5446):1957-9.

37. Tsoukas P, Rapp E, Van Der Kraak L, Weiss ES, Dang V, Schneider C, et al. Interleukin-18 and cytotoxic impairment are independent and synergistic causes of murine virus-induced hyperinflammation. *Blood*. 2020;136(19):2162-74.
38. Landy E, Varghese J, Dang V, Szymczak-Workman A, Kane LP, Canna SW. Complementary HLH susceptibility factors converge on CD8 T-cell hyperactivation. *Blood Adv*. 2023;7(22):6949-63.
39. Chaturvedi V, Marsh RA, Zoref-Lorenz A, Owsley E, Chaturvedi V, Nguyen TC, et al. T-cell activation profiles distinguish hemophagocytic lymphohistiocytosis and early sepsis. *Blood*. 2021;137(17):2337-46.
40. De Matteis A, Colucci M, Rossi MN, Caiello I, Merli P, Tumino N, et al. Expansion of CD4dimCD8+ T cells characterizes macrophage activation syndrome and other secondary HLH. *Blood*. 2022;140(3):262-73.
41. Randall KL, Chan SS, Ma CS, Fung I, Mei Y, Yabas M, et al. DOCK8 deficiency impairs CD8 T cell survival and function in humans and mice. *J Exp Med*. 2011;208(11):2305-20.
42. Schulert GS, Cron RQ. The genetics of macrophage activation syndrome. *Genes Immun*. 2020.
43. Saltzman RW, Monaco-Shawver L, Zhang K, Sullivan KE, Filipovich AH, Orange JS. Novel Mutation in Syntaxin-Binding Protein 2 (STXBP2) Prevents IL-2-induced Natural Killer Cell Cytotoxicity. *The Journal of allergy and clinical immunology*. 2012;129(6):1666.
44. Spessott WA, Sanmillan ML, McCormick ME, Patel N, Villanueva J, Zhang K, et al. Hemophagocytic lymphohistiocytosis caused by dominant-negative mutations in STXBP2 that inhibit SNARE-mediated membrane fusion. *Blood*. 2015;125(10):1566-77.
45. Zhang M, Behrens EM, Atkinson TP, Shakoory B, Grom AA, Cron RQ. Genetic defects in cytolysis in macrophage activation syndrome. *Current rheumatology reports*. 2014;16(9):1-8.
46. Zhang X-Y, Ye X-W, Feng D-X, Han J, Li D, Zhang C. Hemophagocytic lymphohistiocytosis induced by severe pandemic influenza A (H1N1) 2009 virus infection: a case report. *Case reports in medicine*. 2011;2011.
47. Brisse E, Wouters CH, Matthys P. Advances in the pathogenesis of primary and secondary haemophagocytic lymphohistiocytosis: differences and similarities. *Br J Haematol*. 2016;174(2):203-17.
48. Karras A, Thervet E, Legendre C, Groupe Cooperatif de transplantation d'Ile de F. Hemophagocytic syndrome in renal transplant recipients: report of 17 cases and review of literature. *Transplantation*. 2004;77(2):238-43.
49. Poudel A, Lew J, Slayton W, Dharnidharka VR. Bartonella henselae infection inducing hemophagocytic lymphohistiocytosis in a kidney transplant recipient. *Pediatric transplantation*. 2014;18(3):E83-7.
50. Cron RQ, Chatham WW. Development of spondyloarthritis following episodes of macrophage activation syndrome in children with heterozygous mutations in haemophagocytic lymphohistiocytosis-associated genes. *Clin Exp Rheumatol*. 2016;34(5):953.
51. Reiff DD, Cron RQ. Who Would Have Predicted Multisystem Inflammatory Syndrome in Children? *Curr Rheumatol Rep*. 2022;24(1):1-11.
52. Jackson LE, Khullar N, Beukelman T, Chapleau C, Kamath A, Cron RQ, Chatham WW. Prediction of Survival by IL-6 in a Randomized Placebo-Controlled Trial of Anakinra in COVID-19 Cytokine Storm. *Viruses*. 2023;15(10).
53. Cron RQ, Goyal G, Chatham WW. Cytokine Storm Syndrome. *Annu Rev Med*. 2023;74:321-37.
54. Bhatia S, Bauer F, Bilgrami SA. Candidiasis-associated hemophagocytic lymphohistiocytosis in a patient infected with human immunodeficiency virus. *Clin Infect Dis*. 2003;37(11):e161-6.
55. Schulert GS, Zhang M, Husami A, Fall N, Brunner H, Zhang K, et al. Brief Report: Novel UNC13D Intronic Variant Disrupting an NF-kappaB Enhancer in a Patient With Recurrent

Macrophage Activation Syndrome and Systemic Juvenile Idiopathic Arthritis. *Arthritis Rheumatol.* 2018;70(6):963-70.

56. Ruiz-Garcia R, Lermo-Rojo S, Martinez-Lostao L, Mancebo E, Mora-Diaz S, Paz-Artal E, et al. A case of partial dedicator of cytokinesis 8 deficiency with altered effector phenotype and impaired CD8(+) and natural killer cell cytotoxicity. *J Allergy Clin Immunol.* 2014;134(1):218-21.
57. Zhang Q, Davis JC, Lamborn IT, Freeman AF, Jing H, Favreau AJ, et al. Combined immunodeficiency associated with DOCK8 mutations. *The New England journal of medicine.* 2009;361(21):2046-55.
58. Woellner C, Schaffer AA, Puck JM, Renner ED, Knebel C, Holland SM, et al. The hyper IgE syndrome and mutations in TYK2. *Immunity.* 2007;26(5):535; author reply 6.
59. Holland EM, Gonzalez C, Levy E, Valera VA, Chalfin H, Klicka-Skeels J, et al. Case Report: Fatal Complications of BK Virus-Hemorrhagic Cystitis and Severe Cytokine Release Syndrome Following BK Virus-Specific T-Cells. *Front Immunol.* 2021;12:801281.
60. Sakurai T, Kukimoto-Niino M, Kunimura K, Yamane N, Sakata D, Aihara R, et al. A conserved PI(4,5)P2-binding domain is critical for immune regulatory function of DOCK8. *Life Sci Alliance.* 2021;4(4).

Table 1. Demographics, diagnoses, and genetics of HLH patients with heterozygous *DOCK8* mutations.

<u>#</u>	<u>Age</u> [*]	<u>Sex</u>	<u>Disease</u>	<u>Trigger</u>	<u>Mutation</u>	<u>Frequency</u>	<u>Pathogenic</u> [#]
1	Teen	M	Asthma	Bartonella	c.782C>T, p.Ala261Val	novel	likely
2	Teen	M	JIA/ERA	?Flare	c.4850A>G, p.Gln1617Arg	0.1%	possibly
3	Teen	M	T-cell leukemia	?Candida	c.54-1G>T (splice acceptor)	0.03%	likely

* - 13-19 years; # - PolyPhen-2

ERA = enthesitis related arthritis; JIA = juvenile idiopathic arthritis

Table 2. HLH diagnostic features of patients with *DOCK8* mutations.

<u>Criterion/patient</u>	<u>1</u>	<u>2</u>	<u>3</u>
Underlying immunosuppression	No	Yes	Yes
Fever (°F)	103.2	103.8	104.9
Organomegaly (liver/spleen)	hepatosplenomegaly	none	splenomegaly
Cytopenia			
Neutrophil count (<1E9/L)	0.15	4.52	0.00
Platelet count (<100E9/L)	48	176	2
Hemoglobin (<90 g/L)	102	91	47
Aspartate aminotransferase (≥30 U/L)	267	520	134
Triglyceride (≥265 mg/dL)	329	253	1,044
Fibrinogen (<1.5 g/L)	3.6	2.4	5.1
Ferritin (≥500 ng/mL)	1,168	3,706	29,109
NK cell activity (≤2.6 lytic units)	0.6	↓CD107a	ND
Soluble CD25 (≥2,400 U/mL)	5,187	2,075	12,081
Hemophagocytosis	not in marrow	ND	present in marrow
HLH criteria met (≥5 of 8)	7	2	7
HScore (>169)	209 (88-93%)	195 (80-88%)	292 (<99%)
Responsive to anakinra (rhIL-1Ra)	not given	yes	yes

CD25 = interleukin-2 receptor alpha chain; HLH = hemophagocytic lymphohistiocytosis; HScore = reactive hemophagocytic syndrome diagnostic score; ND = not done; NK = natural killer; rhIL-1Ra = recombinant human interleukin-1 receptor antagonist

Fig Legends

FIG 1. Over-expression of CSS patient 1 *DOCK8* mutation diminishes NK cell function. Representative flow cytometry plots (**A, C, E**) and summary bar graphs (**B, D, F**) with means \pm s.d. (n=4) and p values, showing decreased cytotoxicity (**A, B**), decreased degranulation (CD107a expression) (**C, D**), and increased intracellular TNF and IFN γ expression (**E, F**) when NK-92 cells were transfected with FV expressing *DOCK8* c.782C>T compared to WT *DOCK8*.

FIG 2. CSS patient 3 derived *DOCK8* splice acceptor site nucleotide mutation in *DOCK8* intron 1 disrupts RNA splicing in NK-92 cells. **A.** Representations of EGFP-expressing plasmid constructs pEGFP-N1 (left) and pEGFP-Intron (right) with *DOCK8* intron 1 sequence disrupting the EGFP cDNA. **B.** Representative flow cytometry plots of NK-92 cells expressing EGFP 1 day (top) and 3 days (bottom) following transfection with pEGFP-N1 (left, comparator), pEGFP-Intron-WT (middle, WT splice acceptor site control), and pEGFP-Intron-G2T with the patient derived *DOCK8* splice acceptor site mutation (right, c.54-1G>A). **C.** Bar graph summary with EGFP expression means \pm s.d. (n=4) and p values at day 1 and day 3. **D/E/F** A traditional (exon trapping, see Methods) complementary EGFP reporter plasmid approach for assessing RNA splicing is shown to the right.

FIG 3. Stepwise knock-down of endogenous *DOCK8* with siRNA yields decreased NK-92 cell cytotoxicity and degranulation. NK-92 cells were transfected with increasing amounts of *DOCK8*-specific siRNA (or scrambled sequence control, NC). The NK-92 cells were incubated with K562 target cells and representative flow cytometry plots depicting cytolysis (**A**) at 1:1 and 5:1 effector to target cell ratios and summary bar graphs (**B**) with mean cell lysis \pm s.d. (n=3) and p values are shown. Similarly, *DOCK8*-siRNA transfected NK-92 cells were assessed for degranulation (CD107a) in the presence or absence of stimulatory K562 target cells. Representative flow cytometry plots (**C**) and summary bar graphs (**D**) with mean CD107a expression \pm s.d. (n=4) and p values are shown.

FIG 4. Knock-out and reintroduction of *DOCK8* in NK cells with CRISPR/Cas9 demonstrates role of *DOCK8* in NK cell cytolysis. Complete disruption (cutting ctrl) of *DOCK8* in NK-92 cells by CRISPR/Cas9 diminishes NK-92 cell cytotoxicity (K562 cells) and degranulation (CD107a expressions). Reintroduction by homology-directed repair (HDR) of WT *DOCK8* (782C), but not patient 1 mutation (782T), partially restores NK cell function. Representative flow cytometry plots of cell lysis (**A**) and degranulation (**C**) and summary bar graphs of mean cell lysis (**B**) and mean CD107a expression (**D**) \pm s.d. (n=4) with p values are shown.

FIG 5. *Dock8*^{-/-} mice infected with LCMV experience increased hyperinflammation relative to wild-type controls. Wild-type (WT) and *DOCK8* deficient mice (*Dock8*^{-/-}) were infected with 2×10^6 PFU of LCMV intraperitoneally. **(A)** Daily weights expressed as % of initial body weight, error bars represent s.d. **(B)** Splenic weight normalized to total body weight, analyzed by t-test, ** – p <0.01. **(C)** Splenocytes were stained in multicolor flow cytometry for the listed markers, and percent of total splenocytes for each population is presented. **(D)** White blood cell count (WBC), red blood cell count (RBC), and platelet count (PLT) were analyzed from cheek bled peripheral blood pre-infection (day 0) and day 8 post infection. Counts were obtained using a Sysmex XT-2000iV Hematology Analyzer. Analyzed for genotype x disease interaction by two-way ANOVA, ** - p <0.01. b Serum IFN γ and sCD25 were measured by ELISA on day 8 post

infection, analyzed by t-test. **(F)** Viral burden, analyzed by Vero cell plaque assay from splenic lysates, analyzed by t-test, * – $p < 0.05$.

FIG 6. Despite driving T-cell lymphopenia, *Dock8* deficiency interacts with excess IL-18 to amplify CD8 T-cell activation and LCMV-induced HLH. Littermate mice of the indicated genotypes were assessed at 8-10 weeks of age for **(A)** spontaneous splenomegaly, splenic NK cell abundance, and the number and activation state of splenic CD4 and CD8 T-cells. Separately, mice of the same genotypes were infected with LCMV and assessed at Day 8-9 post infection for **(B)** weight loss, neutrophilia, anemia, and number and activation state of splenic CD8 T-cells. Data were analyzed by two-way ANOVA for significant differences based on *Dock8* genotype, presence of *I118* transgene, and interaction. For bar graphs, ANOVA results indicate comparisons of the % of CD4 or CD8 T-cells that were PD1+. NS=not significant, indicating $p > 0.2$.

FIG E1. Patient 1 *DOCK8* mutation has no effect on granzyme B expression. NK-92 cells were analyzed by FCM in the presence (+) or absence (-) of K562 cells for intracellular granzyme B expression (2nd row from top) in comparison to APC-conjugated isotype control antibody (top row). WT (3rd row from top) or *DOCK8* mutant (c.782T) (bottom row) FV transfected NK-92 cells were assessed for granzyme B expression in a similar fashion. MFI and percentage positive cells are reported on each FCM plot (side scatter on y-axis, APC detection on x-axis), and data shown are representative of 4 independent experiments.

FIG E2. Patient 1 *DOCK8* mutation modestly diminishes NK-92 cell and K562 cell conjugation. WT (c.782C) or patient 1 *DOCK8* mutation (c.782T) FV transfected NK-92 cells (co-expressing EGFP, y-axis) were co-incubated 1:1 with K562 target cells (labeled with eFluor 670 and detected by APC emission wavelength, x-axis) for 0, 10, 30, or 60 minutes. FCM plots depicting NK-92 cells binding as a percentage of K562 cells (top rows), or K562 cells binding as a percentage of NK-92 cells are presented (middle rows). The upper right quadrants in the bottom rows show the percentages of NK-92 cell to K562 cell conjugates with quadrant percentages listed. Data shown are representative of 4 independent experiments.

FIG E3. Over-expression of CSS patient 2 *DOCK8* mutation diminishes NK cell function. Representative flow cytometry plots **(A, C)** and summary bar graphs **(B, D)** with means \pm s.d. ($n=4$) and p values, showing decreased cytotoxicity **(A, B)** and decreased degranulation (CD107a expression) **(C, D)** when NK-92 cells were transfected with FV expressing *DOCK8* c.4850A>G compared to WT *DOCK8*.

FIG. E4. Pathology of *Dock8*^{-/-} mice infected with LCMV demonstrate increased hepatic endothelial cell activation. Mice were infected with LCMV as in Fig 5. Livers were harvested on day 8 and were assessed by a blinded pathologist and scored for various features. **(A)** Lobular inflammatory score as measured by number of inflammatory foci per 100x field in the most involved area. **(B)** Portal inflammatory score as measured on a scale of 0-4 with 0 being absent and 4 representing severe inflammation. **(C)** Histologic endothelial activation as measured by morphologic changes in the vascular endothelial cells was 0-4 with 0 being normal and 4 representing severe changes of rounding of cells, plumpness of cytoplasm and enlargement of nuclei. **(D)** Representative histomicrographs of livers from WT and *Dock8*^{-/-} mice showing complete occlusion of venules by inflammatory cells in *Dock8*^{-/-} mice.

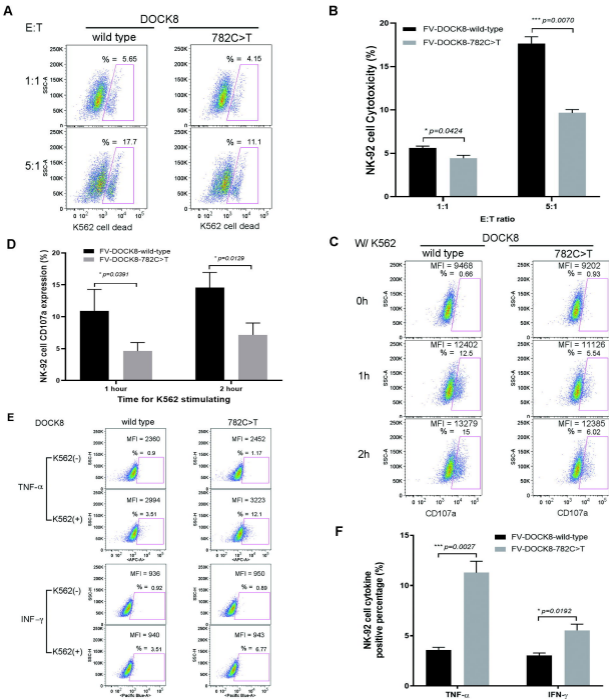


Fig 1

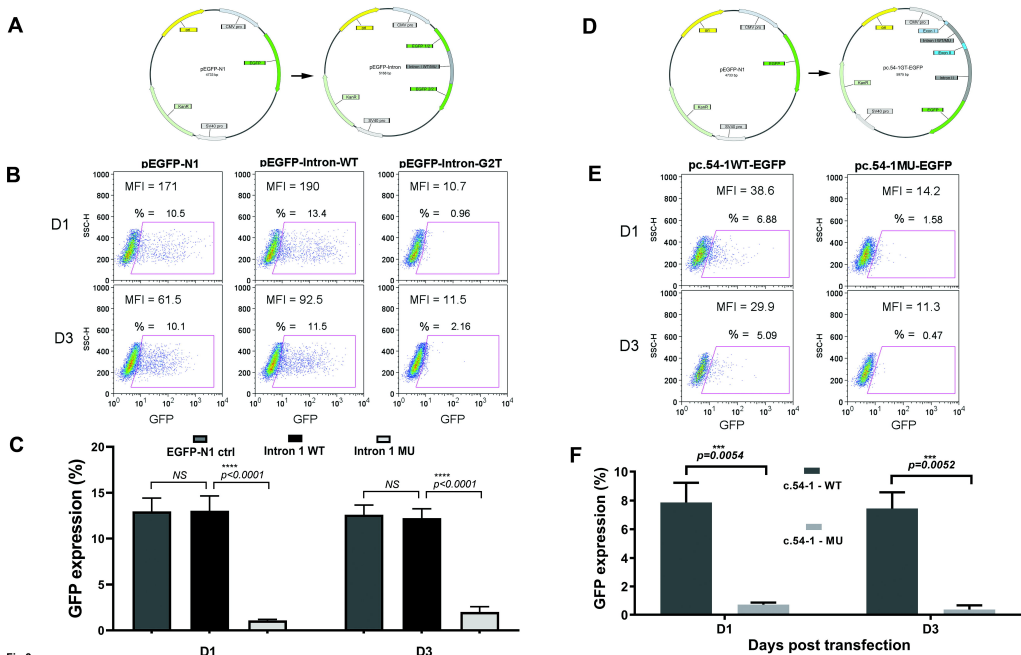


Fig 2

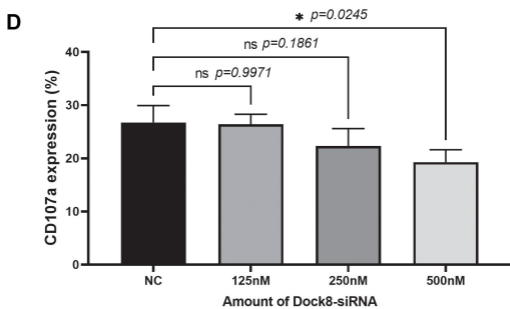
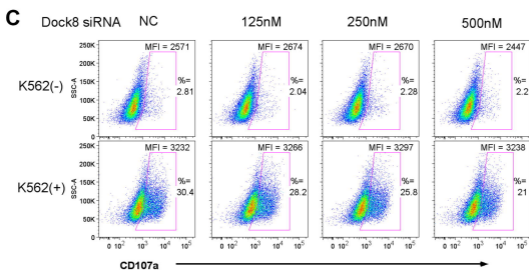
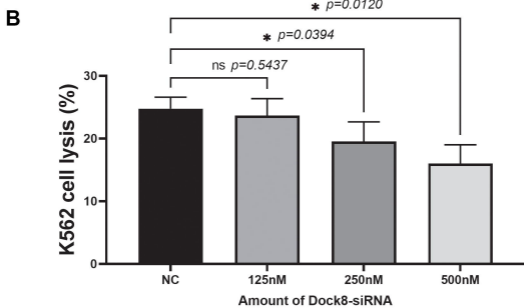
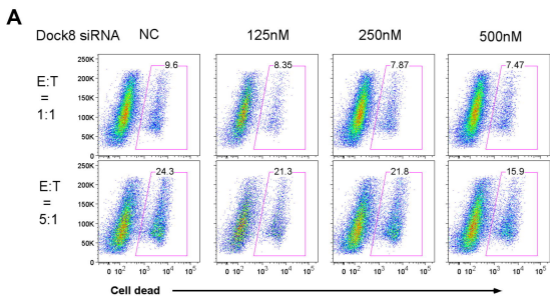


Fig 3

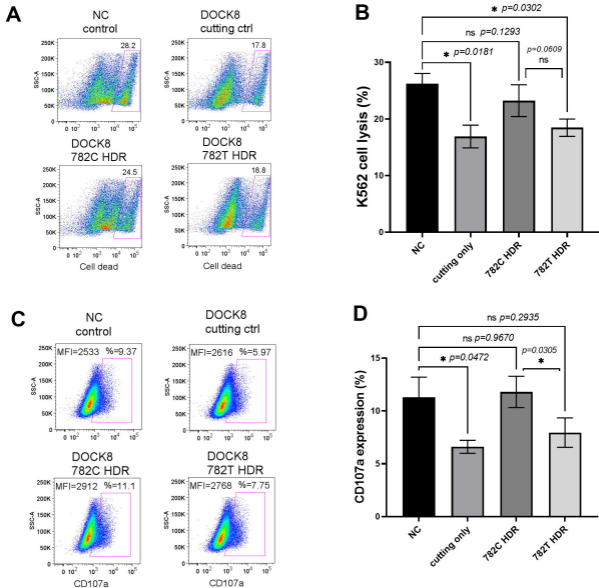


Fig 4

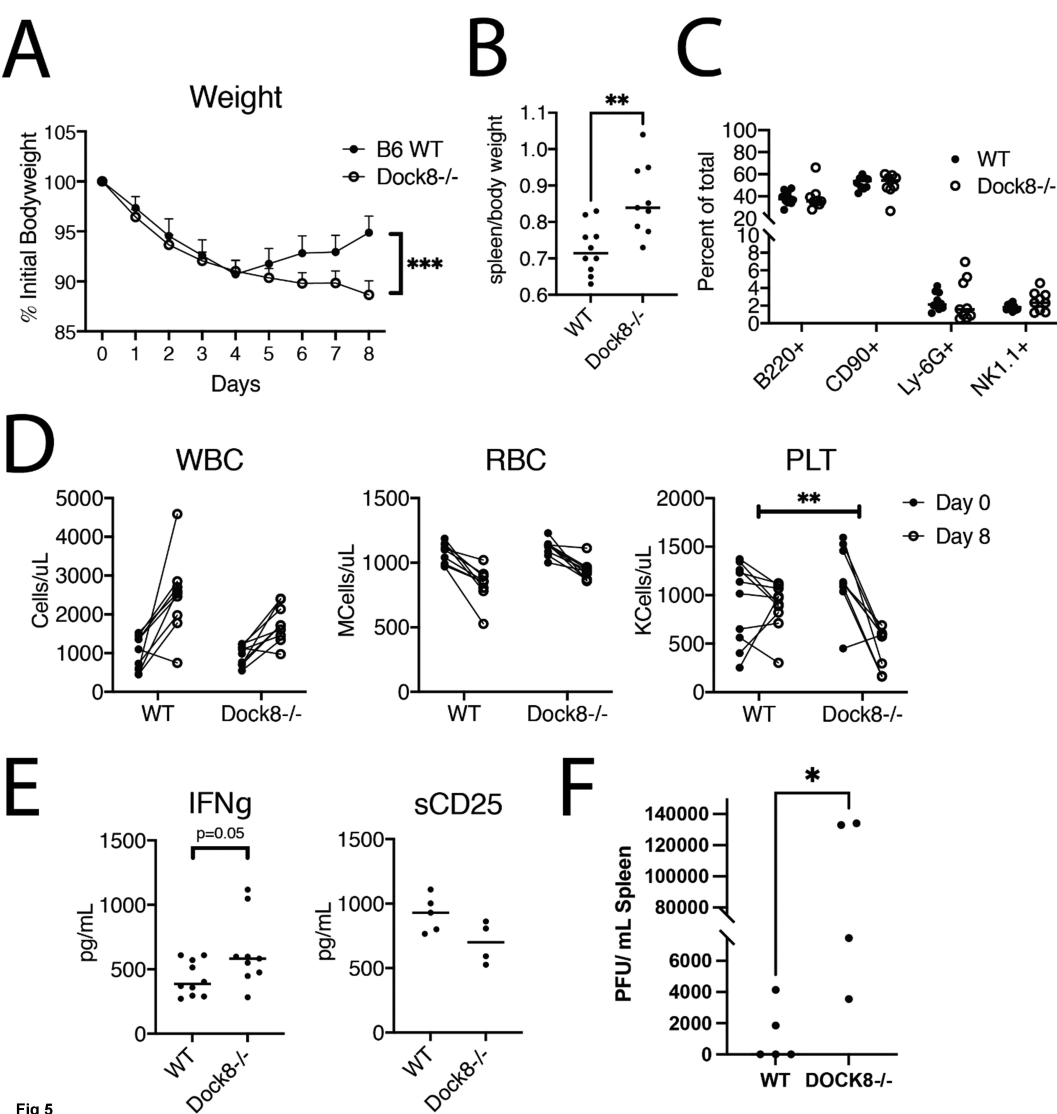
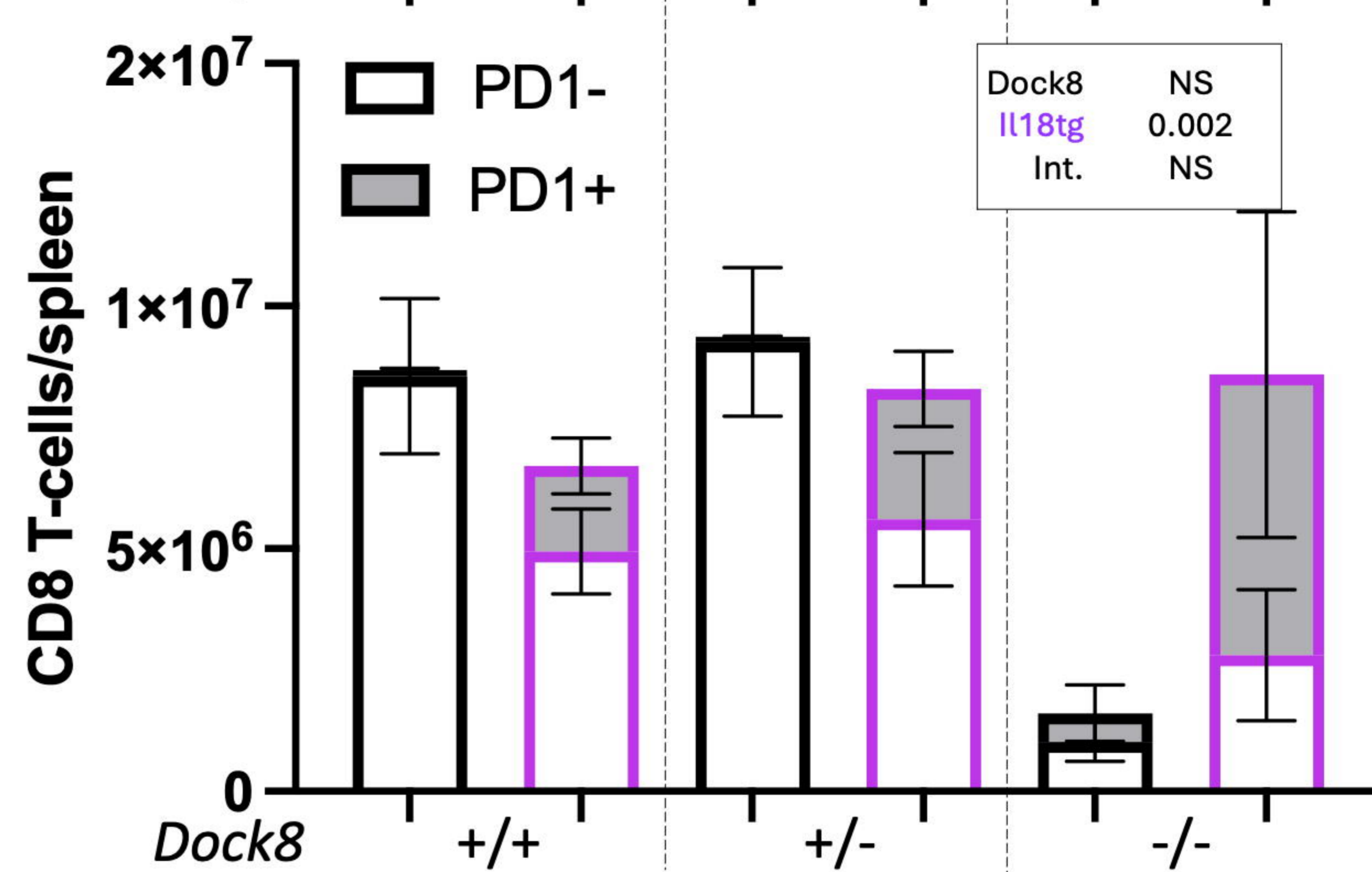
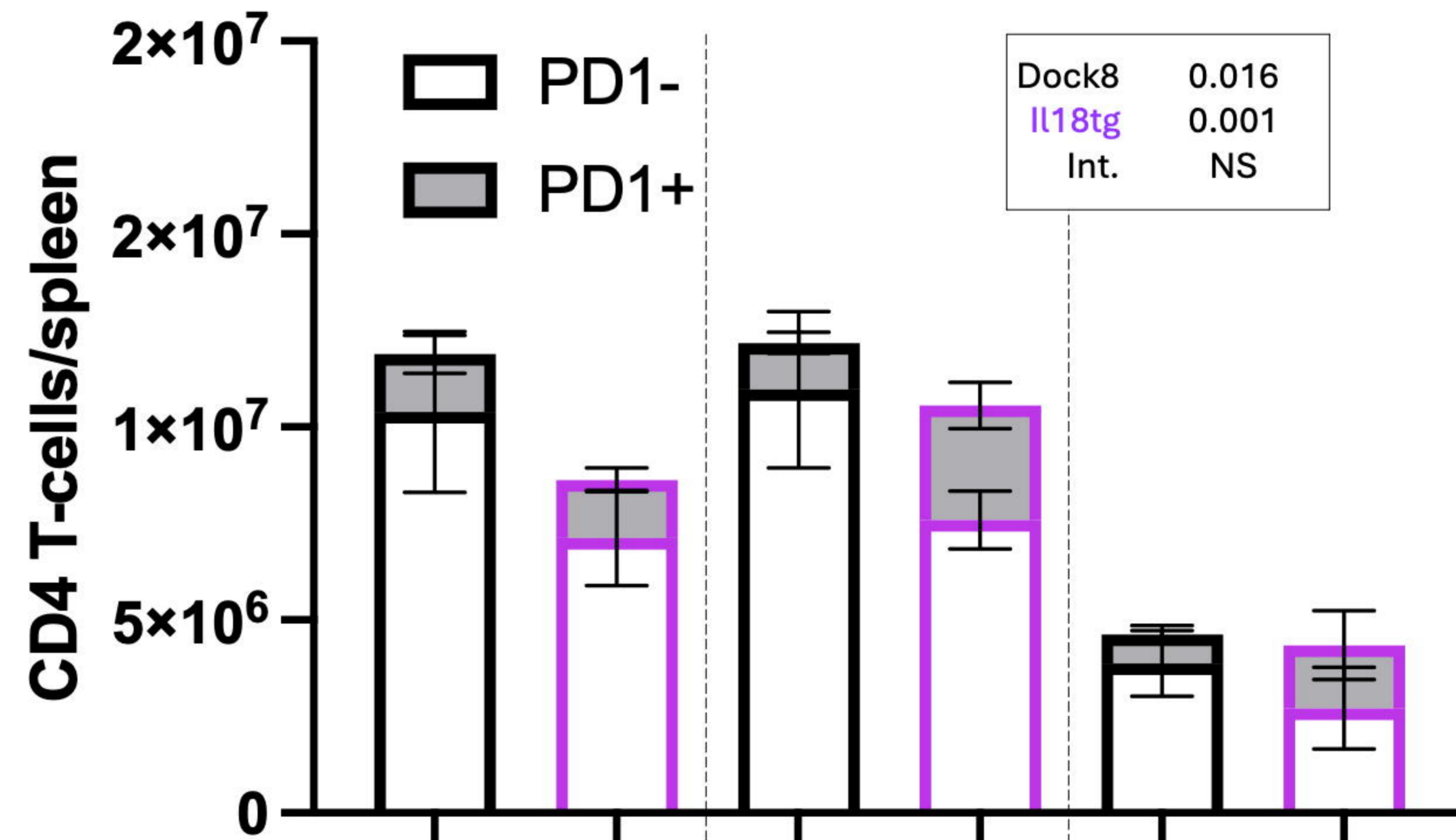
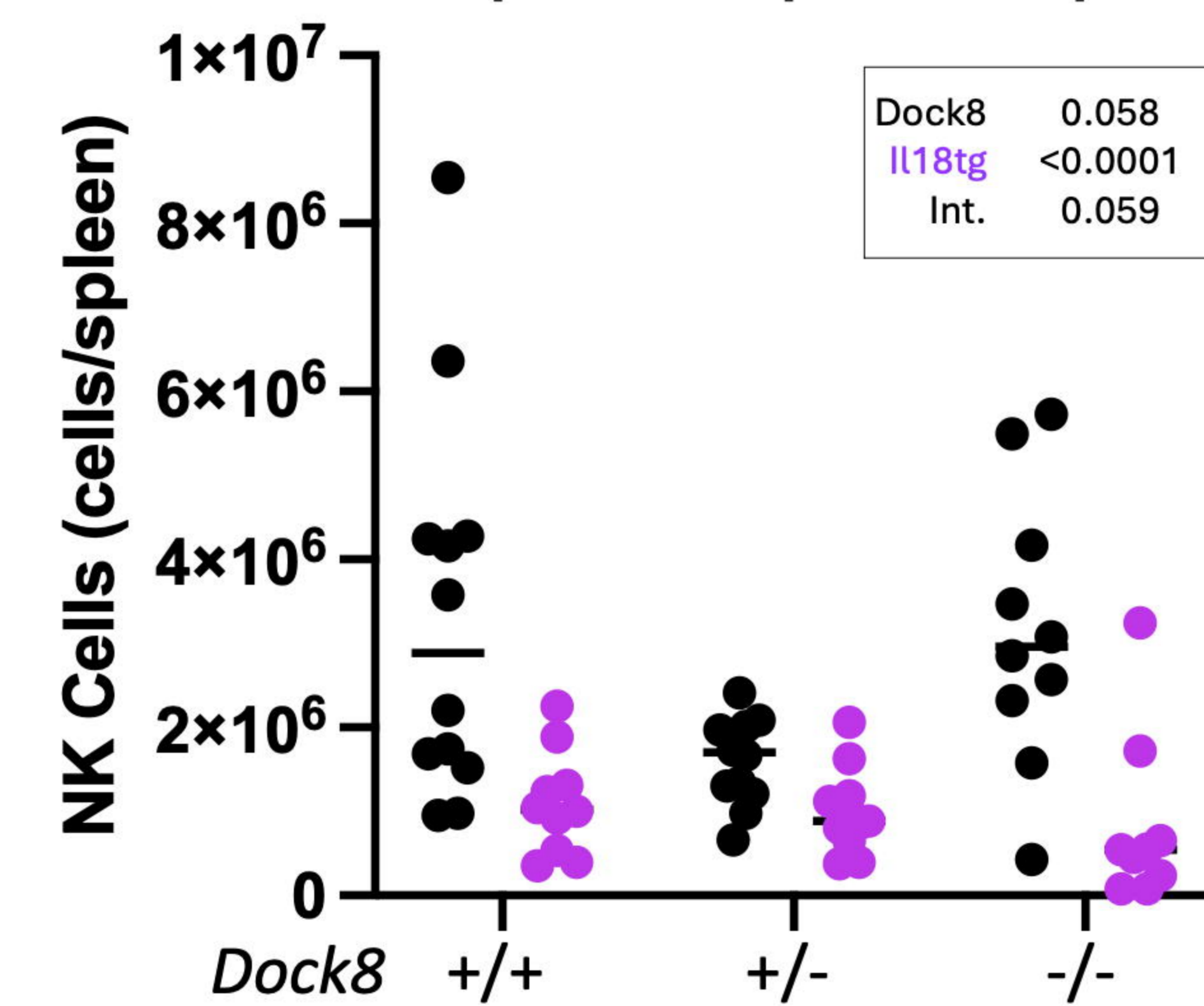
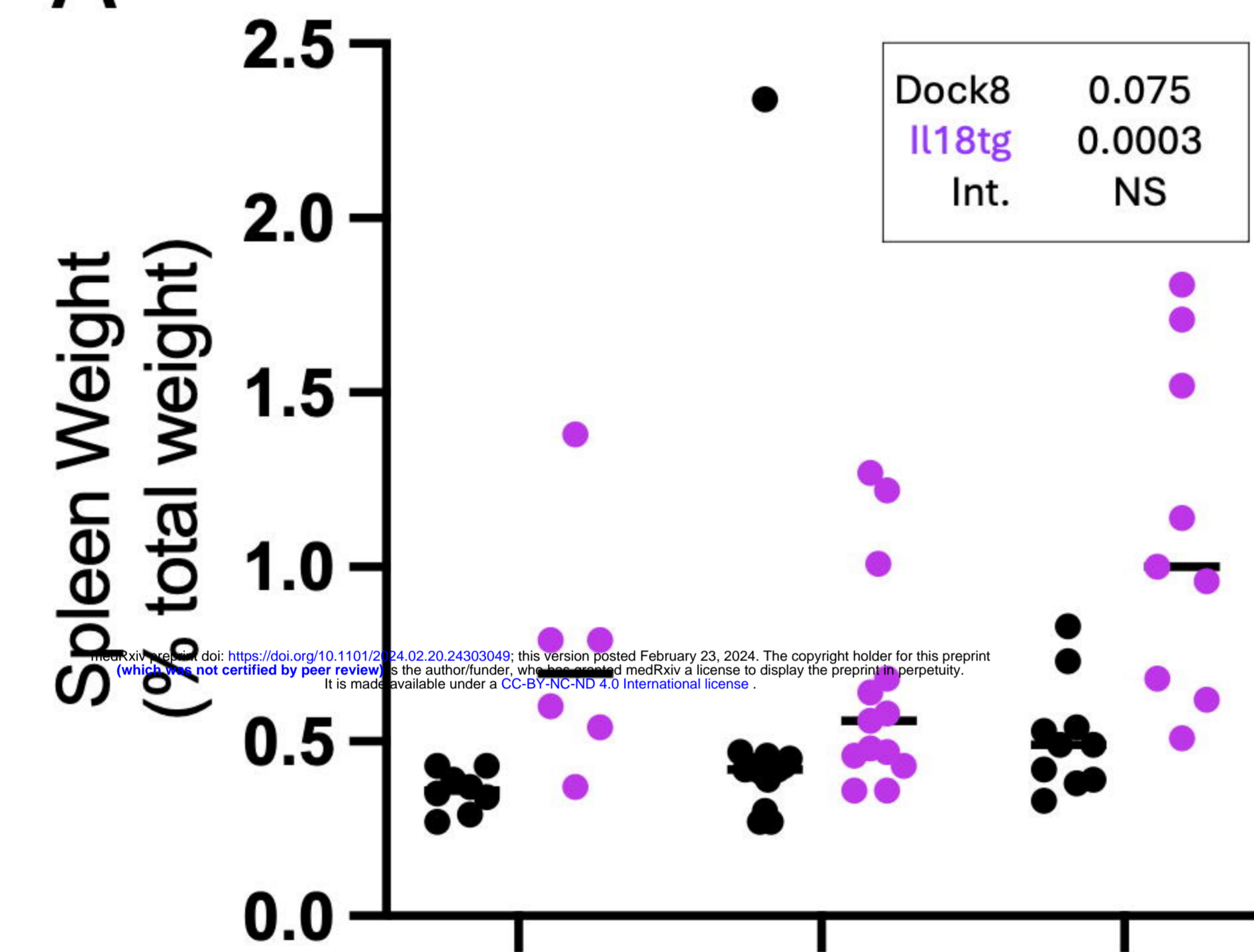
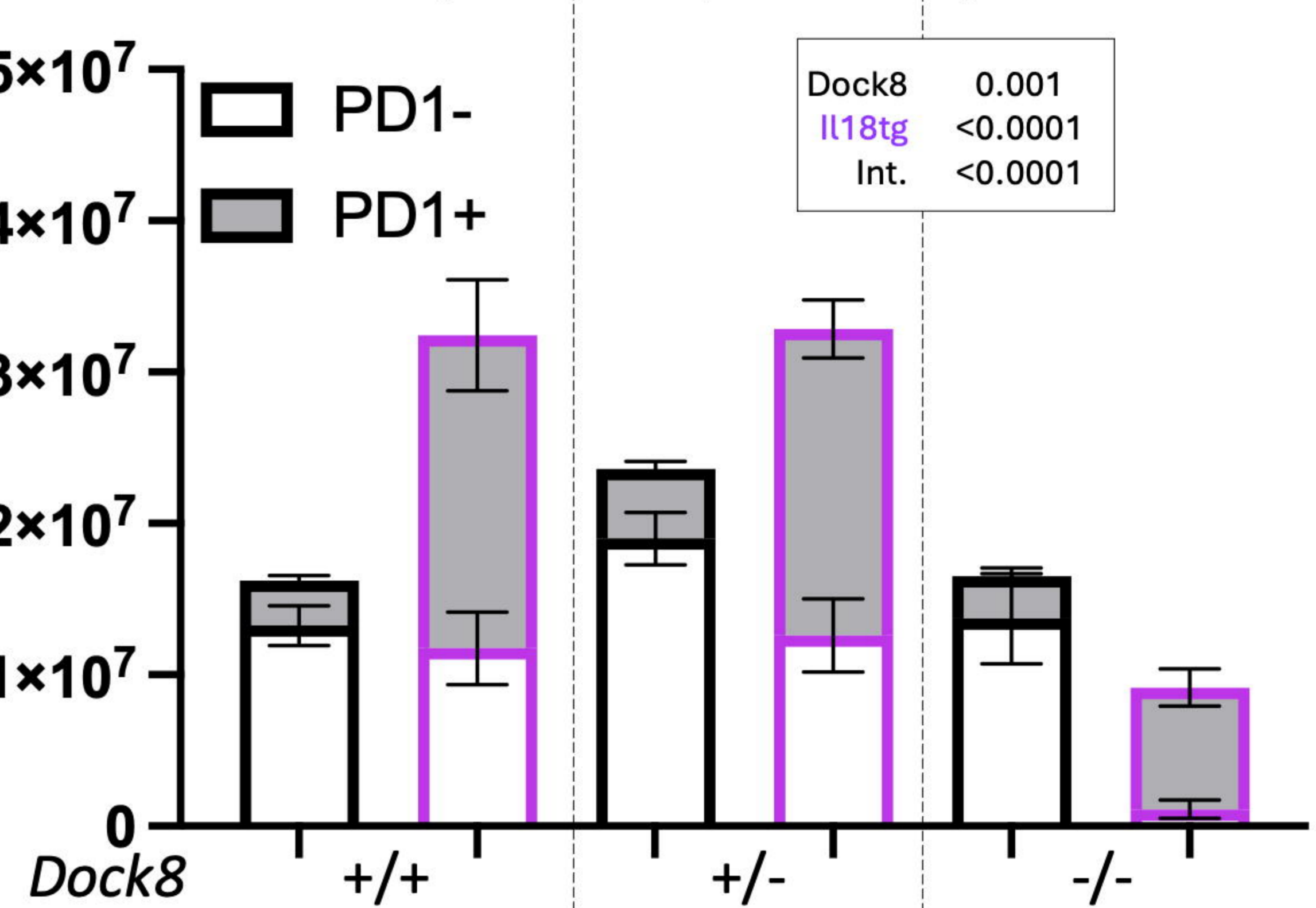
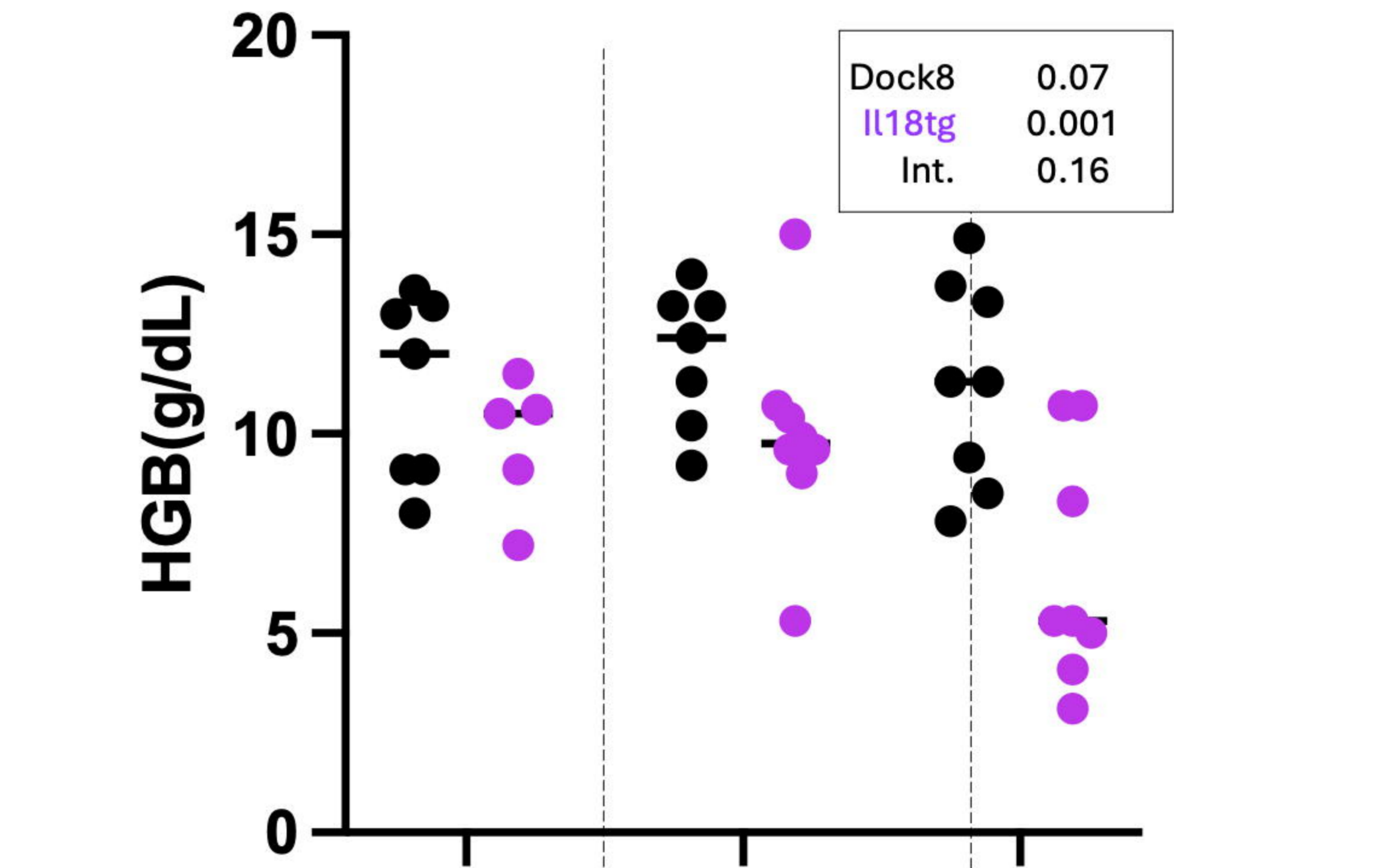
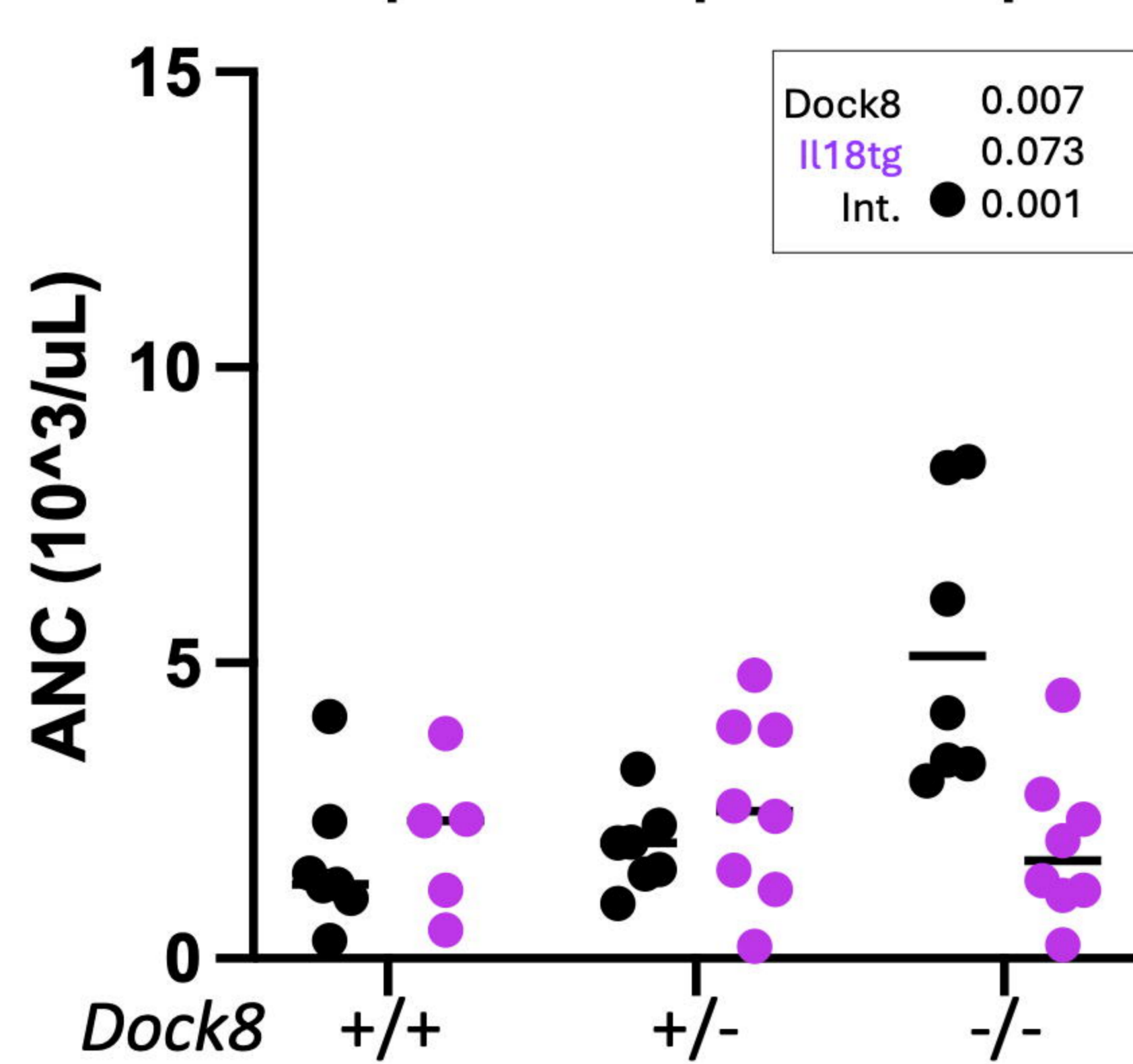
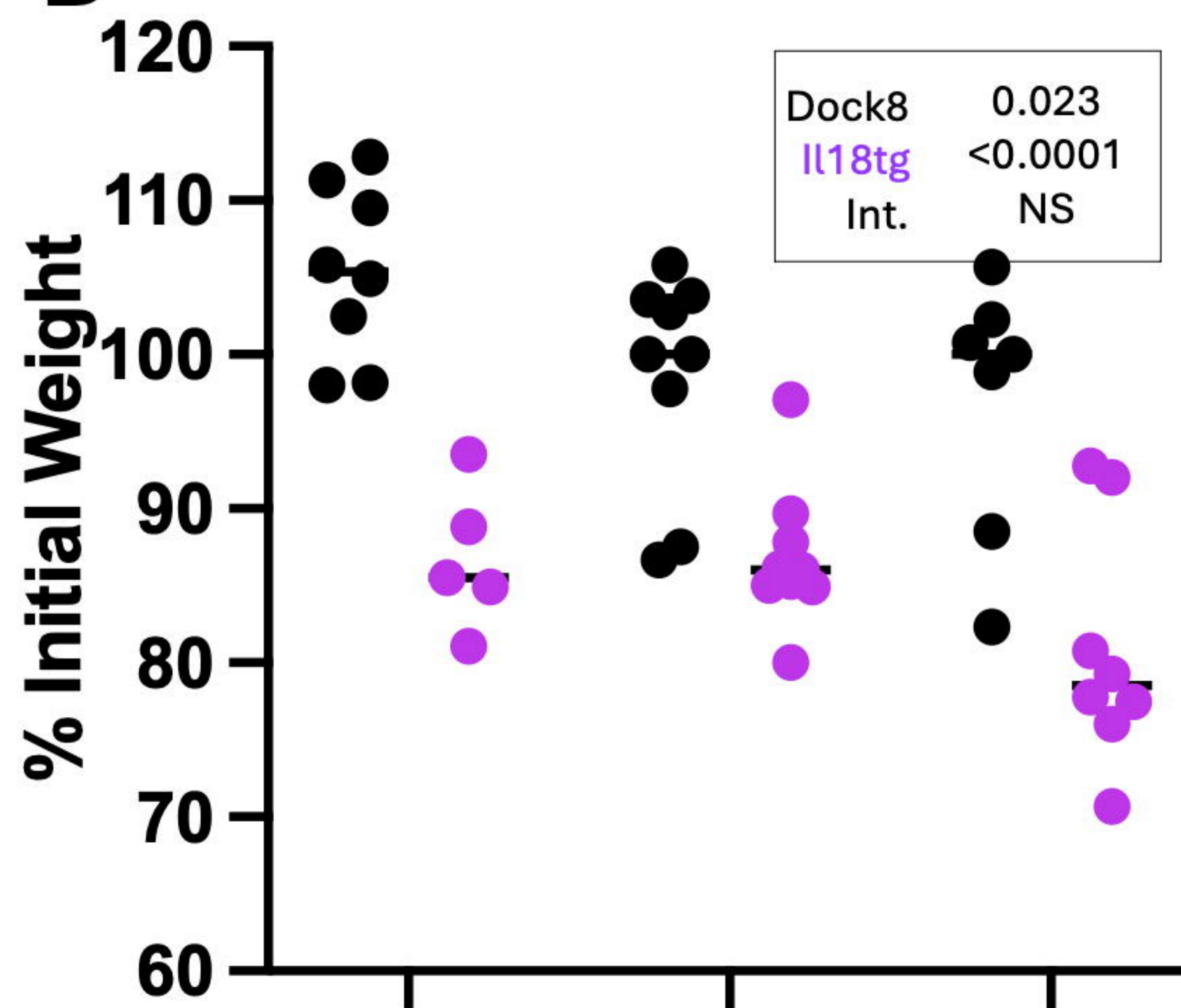


Fig 5

A**B**

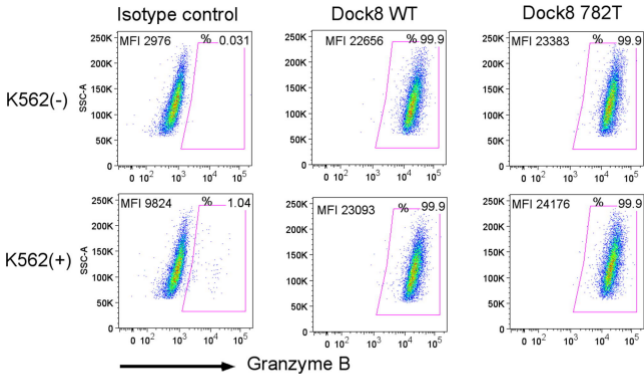


Fig E1

DOCK8

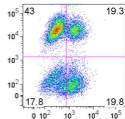
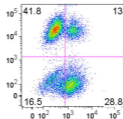
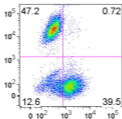
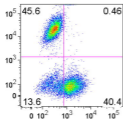
0 mins

10 mins

30 mins

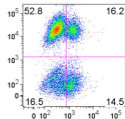
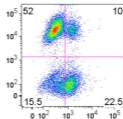
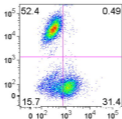
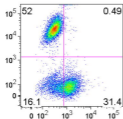
60 mins

WT



782T

K562-AF747



NK-92-GFP

Fig E2

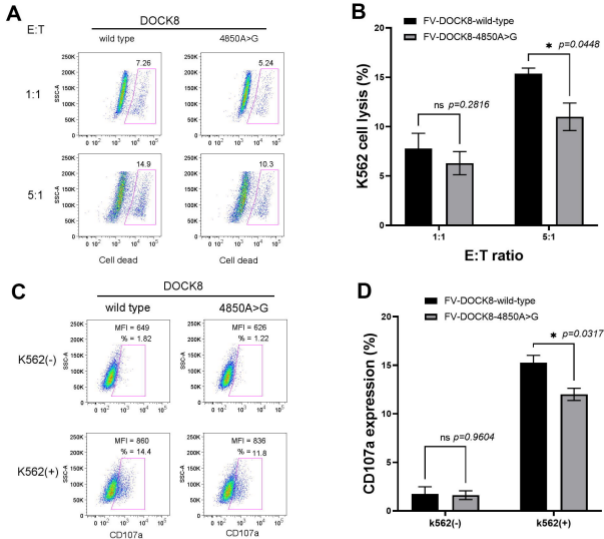


Fig E3

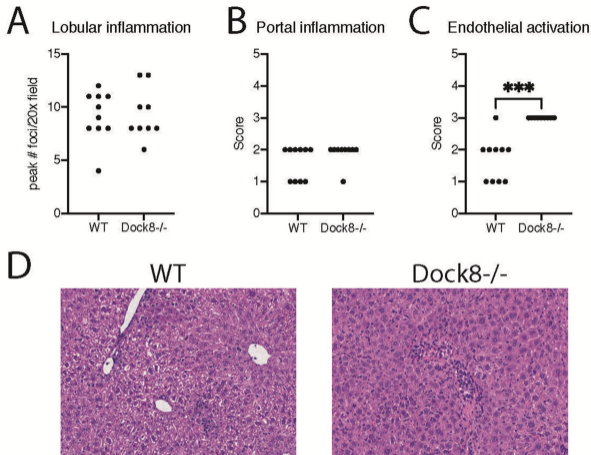


Fig E4